Diagnostic Accuracy of Glaucoma With Sector-Based and a New Total Profile–Based Analysis of Neuroretinal Rim and Retinal Nerve Fiber Layer Thickness

Vishva M. Danthurebandara, Jayme R. Vianna, Glen P. Sharpe, Donna M. Hutchison, Anne C. Belliveau, Lesya M. Shuba, Marcelo T. Nicolela, and Balwantray C. Chauhan

Department of Ophthalmology and Visual Sciences, Dalhousie University and Nova Scotia Health Authority, Halifax, Nova Scotia, Canada

Correspondence: Balwantray C. Chauhan, Department of Ophthalmology and Visual Sciences, Dalhousie University, 1276 South Park Street, 2W Victoria, Halifax, Nova Scotia, Canada B3H 2Y9; bal@dal.ca.

Submitted: July 29, 2015
Accepted: December 8, 2015

Citation: Danthurebandara VM, Vianna JR, Sharpe GP, et al. Diagnostic accuracy of glaucoma with sector-based and a new total profile–based analysis of neuroretinal rim and retinal nerve fiber layer thickness. *Invest Ophthalmol Vis Sci*. 2016;57:181–187. DOI:10.1167/iovs.15-17820

Purpose. To compare the diagnostic accuracy of conventional sector-based analysis with a method devised to detect the smallest localized neuroretinal rim and retinal nerve fiber layer thickness (RNFLT) damage.

Methods. One eye of 151 glaucoma patients and 83 healthy controls (median age and MD, 71.7 and 66.7 years, and −3.6 and −0.3 dB, respectively) was imaged with spectral-domain optical coherence tomography (OCT). Bruch's membrane opening-minimum rim width (BMO-MRW) and RNFLT were determined at 1° intervals and also averaged for each sector. A classification of glaucoma was made with sectoral analysis when the sectoral value was below the 1%, 5%, or 10% normative limit (from an independent normative dataset); and with total analysis when a given number of measurements was below the 1%, 5%, or 10% normative limit.

Results. With the 1% normative limit, BMO-MRW sectoral analysis yielded sensitivity of 87% and specificity of 92%; while at the same specificity (92%), total analysis yielded sensitivity of 88%. With RNFLT, sectoral analysis yielded sensitivity of 85% and specificity of 95%; while at the same specificity (95%), total analysis yielded sensitivity of 83%. The results for the 5% and 10% normative limits yielded lower specificity but higher sensitivity. In the whole glaucoma population, none of the sensitivity values of the sectoral and total analysis at the same specificities were statistically different.

Conclusions. The diagnostic accuracy of sectoral analysis was equivalent to total analysis. These results indicate that BMO-MRW and RNFLT defects were wide and deep enough for detection by conventional sectoral analysis.

Keywords: diagnostic accuracy, neuroretinal rim, retinal nerve fiber layer

Spectral-domain optical coherence tomography (OCT) is a valuable tool for the diagnosis and management of several eye diseases. In glaucoma, the high-resolution images obtained with OCT allow clinicians to visualize pertinent anatomical features of the optic nerve head (ONH)[1–4] and compute neuroretinal rim parameters that are anatomically and geometrically accurate. One such approach is the shortest distance from Bruch's membrane opening (BMO), the maximum aperture in the anterior ONH through which retinal ganglion cell axons can pass through to exit the eye,[5] to the internal limiting membrane.[6–8] This parameter, termed BMO-minimum rim width (BMO-MRW), has been shown by us and others to yield better diagnostic accuracy[9] and better correlation to the visual field[10–13] compared with traditional disc margin based rim measures.

Parameters such as BMO-MRW and peripapillary retinal nerve fibre layer thickness (RNFLT) are frequently reported as global or sectoral means. The number and size of sectors is not standardized,[14–17] however, four 40° sectors (superior-temporal, inferior-temporal, superior-nasal, and inferior-nasal), one 90° temporal sector, and one 110° nasal have been used in several studies.[6,14,18] While global means summarize the entire neuroretinal rim and RNFL, localized loss may escape detection as it could have a negligible impact on the global mean. Sectoral means are more likely to capture localized damage and studies have confirmed that this approach may be more accurate than using only global means.[19–21] However, the diagnostic accuracy of a sector-based analysis depends on the width and severity of localized damage relative to sector size. For example, a localized rim or RNFL defect of a given size and depth will have a larger influence on the sector mean in a small sector compared with a large sector. Moreover, a localized defect that straddles two sectors could have a relatively small effect on the respective sector means and escape detection. Relatively little research exists on how the accuracy of glaucoma diagnosis depends on sector size.[17,22,23]

The purpose of the current study was to determine how well conventional sector-based analysis is able to capture localized rim or RNFL defects. We propose an analysis that captures the smallest possible localized defect and compare its diagnostic capability with that of conventional sector-based analysis. Additionally, because the size and width of localized defects depend on glaucoma severity, we determined the impact of the level of visual field damage on the use of these two diagnostic approaches.

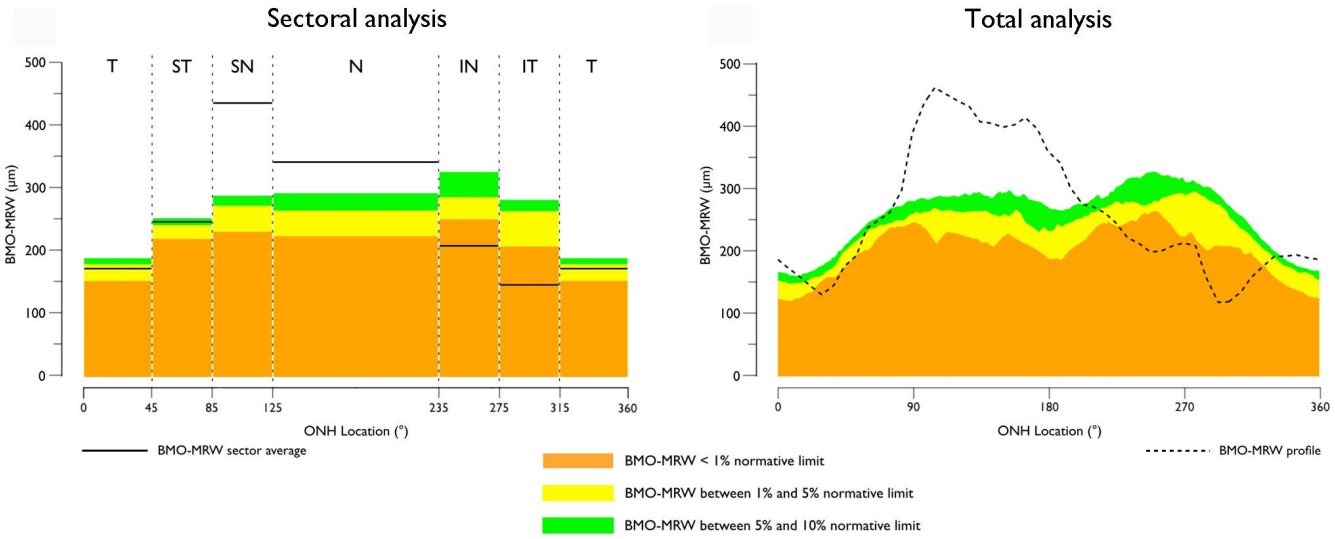

Figure 1. Sectoral (*left*) and total (*right*) analysis of BMO-MRW of a glaucoma patient. *Horizontal black lines* represent the sectoral BMO-MRW values for the patient (*left*). A classification of abnormality occurred when the average sectoral value was below the corresponding normative limit for in least one sector. In this example, the average sector values in the inferior nasal and inferior temporal quadrants were below the 1% normative limit. *Dashed black line* represents the BMO-MRW profile for the same patient (*right*). Total analysis is based on the number of individual locations that are below the 1% normative limit. T, temporal; ST, superior-temporal; SN, superior-nasal; N, nasal; IN, inferior-nasal; IT, inferior-temporal.

Methods

Participants

Open-angle glaucoma patients and healthy control subjects were recruited from two ongoing longitudinal observational studies at the Eye Care Centre, Nova Scotia Health Authority, Halifax, Nova Scotia, Canada.

Inclusion criteria for patients when the longitudinal studies were initiated were: (1) visual field damage, characteristic of open angle glaucoma, with MD between −2 and −10 dB, when first recruited for the longitudinal studies, (2) clinical appearance of glaucomatous cupping and/or localized notching of the neuroretinal rim, (3) best-corrected visual acuity of at least 6/12, and (4) pupil diameter of at least 3 mm. Exclusion criteria were: (1) nonglaucomatous ocular disease and systemic disease or systemic medication known to affect the visual field or ability to participate in the study, (2) chronic ocular medication other than for glaucoma, (3) distance refraction not exceeding 6.00 diopters (D) equivalent sphere and 3.00 D of astigmatism, and (4) contact lens wear.

Inclusion criteria for controls when the longitudinal studies were initiated were: (1) normal clinical eye examination with an IOP less than 21 mm Hg, and (2) a normal visual field defined as a Glaucoma Hemifield Test, MD, and pattern standard deviation within normal limits. The exclusion criteria were: (1) distance refraction not exceeding 6.00 D equivalent sphere and 3.00 D of astigmatism, and (2) contact lens wear.

If both eyes were eligible, one eye was randomly selected as the study eye. The study adhered to the tenets of the declaration of Helsinki and was approved by the Research Ethics Board of the QE-II Health Science Centre. All participants gave written informed consent.

Procedures

The ONH and the peripapillary RNFL were imaged with OCT (Spectralis; Heidelberg Engineering GmbH, Heidelberg, Germany). Scans were acquired according to the subject's specific fovea-BMO axis, and data subsequently sectorized according to this axis[24] to minimize the geometrical errors introduced by conventional image acquisition.[25,26] Two scan patterns were used. First, a pattern with 24 radially equidistant 15° B-scans. Each radial B-scan was averaged from 20 to 30 individual scans with 1536 A-scans per B-scan. The BMO points and inner limiting membrane (ILM) were segmented in each B-scan with automated software.[27] Manual corrections were made when necessary. Bruch's membrane opening–MRW, the minimum distance between BMO and ILM, was calculated at the two points in each B-scan. Second, a circular scan along a peripapillary circle of 3.5-mm diameter to measure RNFLT. Data were averaged from 16 individual circular B-scans, each comprising 1536 A-scans. For the current study the most recent OCT scan of each participant and corresponding visual field test was selected for analysis. We consulted the research and clinical charts of all study patients to verify that the inclusion and exclusion criteria were satisfied.

Data Analysis and Statistical Methods

The B-scans yielded BMO-MRW estimates at each radial scan position, that is, at every 7.5° around the ONH. Values at each degree were linearly interpolated, yielding 360 measurements. Retinal nerve fiber layer thickness was measured in 768 locations around the 3.5-mm scan circle and were similarly interpolated to yield 360 measurements. All data were converted to right-eye format. Bruch's membrane opening–MRW and RNFLT values were computed as means for four 40° sectors (superior-temporal [45°–85°], inferior-temporal [275°–315°], superior-nasal [85°–125°], and inferior-nasal [235°–275°]), one 90° sector (temporal [315°–45°]) and one 110° sector (nasal [125°–235°]).

In the current research, we used two types of analyses: the conventional sectoral analysis and a method devised by us termed total analysis.

In sectoral analysis, each sector was analyzed independently. We compared each individual mean sectoral value with the corresponding sectoral normal limit and classified BMO-MRW or RNFLT as abnormal if the value was below the corresponding sectoral normal limit (see below) in an independent normative database.[24] Any individual with at least one sector outside normal limits was classified as having glaucomatous

Table 1. Summary Statistics of Study Subjects

	Glaucoma Patients	Healthy Controls	*P* Value
Age, y	71.7 (64.9 to 78.1)	66.7 (62.7 to 76.1)	0.05
MD, dB	−3.6 (−7.7 to −1.7)	−0.3 (−1.1 to 0.8)	0.00
Global BMO-MRW, μm	180.3 (148.3 to 220.8)	293.1 (261.7 to 333.5)	0.00
Global RNFLT, μm	67.3 (60.2 to 78.2)	94.8 (87.9 to 103.6)	0.00

Values shown are medians (interquartile range).

damage. Figure 1 illustrates how classifications for the sectoral analysis were derived.

In total analysis, BMO-MRW and RNFLT values at each measurement point were analyzed independently. We compared the value at each measurement point with the corresponding normal limits (see below). The number of measurement points with a value below the corresponding normative limit was computed to classify an eye as having glaucomatous damage. Figure 1 illustrates how classifications for the total analysis were derived.

We used the 1%, 5%, or 10% normative limits from the independent OCT normative database[24] as cut-off to classify a subject as having glaucomatous damage. Due to the dependency of the normative limits on age and BMO size (BMO area and BMO radius), the normative limits were first adjusted for these parameters and then applied to classify individual eyes as normal or glaucoma.

The Mann-Whitney *U* test was used to compare group variables. Diagnostic performances of BMO-MRW and RNFLT were assessed with a receiver operating characteristic (ROC) analysis for both sectoral and total analyses. With sectoral analysis, sensitivity, and specificity were calculated for the 1%, 5%, and 10% normative limits. Therefore, there was one discrete point for sectoral analysis on the ROC curve for a given normative limit, whereas with total analysis sensitivity and specificity were computed for all possible cut-off values, that is, the number of measurement points with parameter values below the corresponding normative limit. Sensitivity obtained with sectoral analysis was compared with that with total analysis obtained at the same level of specificity with the McNemar test for correlated proportions.[28] The analysis was first performed on all the study participants. It was then performed with glaucoma patients divided into two groups based on disease severity based on visual field damage with a median split in MD: patients with MD greater than or equal to −3.6 dB (Group 1) and patients with MD less than −3.6 dB (Group 2). Data analysis was performed with the open-source software R.[29]

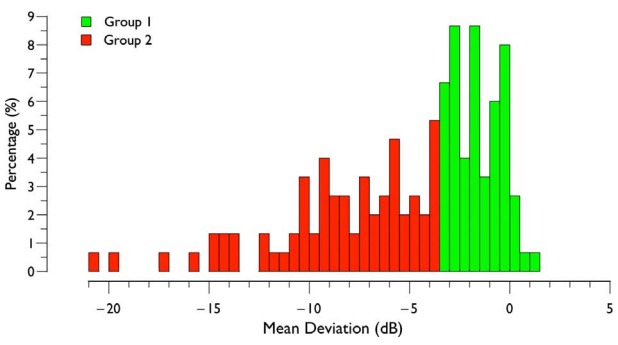

Figure 2. Distribution of visual field MD in glaucoma patients. Data are divided (Group 1 and Group 2) according to the median split in MD.

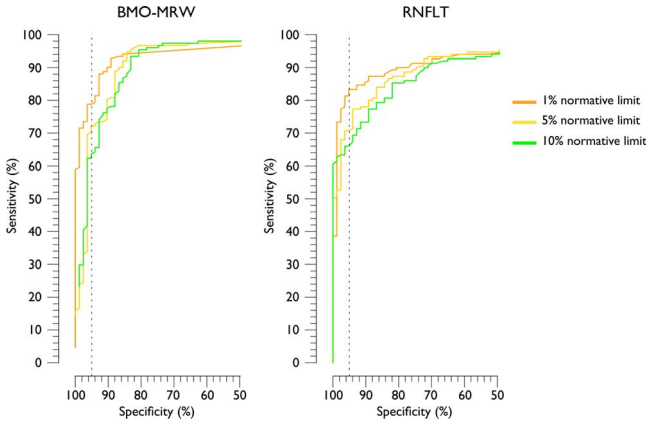

Figure 3. ROC curves of total analysis of BMO-MRW (*left*) RNFLT (*right*). ROC curves are based on all possible cut-off values for the parameters and are shown for the 1%, 5%, and 10% normative limits.

Results

There were 151 glaucoma patients and 83 healthy controls in the study. Their median (interquartile range) age, MD and summary OCT parameters are shown in Table 1. There was a statistically significant difference between patients and controls for all the parameters investigated ($P < 0.01$) except age, which was marginally higher in patients ($P = 0.05$). The distribution of MD in Group 1 and Group 2 glaucoma patients is shown in Figure 2.

In total analyses, both BMO-MRW and RNFLT yielded higher diagnostic performance ($P < 0.04$) with the 1% normative limit compared with the 5% and 10% normative limits (Fig. 3). With BMO-MRW, sensitivity at 95% specificity at the 1%, 5%, and 10% normative limits was 79%, 71%, and 63%, respectively. The corresponding figures for RNFLT were 83%, 70%, and 66%, respectively (Fig. 3).

Sectoral analysis had diagnostic performance equivalent to the corresponding total analysis. With the 1% normative limit, sectoral analysis with BMO-MRW yielded sensitivity of 87% and specificity of 92%. At the same specificity (92%), total analysis had a sensitivity of 88% ($P = 0.24$ compared with sectoral analysis; Fig. 4A and Table 2). With the 1% normative limit, sectoral analyses with RNFLT yielded 85% sensitivity and 95% specificity. At the same specificity (95%), total analysis had a sensitivity of 83% ($P = 0.54$ compared with sectoral analysis; Fig. 5A and Table 3). Similar results were obtained with 5% and 10% normative limits and are summarized in Tables 2 and 3.

Because all healthy subjects were used for computing specificity, the specificity value was identical for the analysis of all, and Group 1 and Group 2 patients. Similar to the analysis with all patients, sectoral and total analyses with Group 1 showed equivalent diagnostic performance. With the 1% normative limit, sectoral analysis with BMO-MRW had sensitivity of 80% and specificity of 92%. At the same specificity (92%), total analysis yielded 81% sensitivity ($P = 0.96$ compared with sectoral analysis; Fig. 4B and Table 2). With the 1% normative limit, sectoral analyses with RNFLT had 75% sensitivity and 95% specificity. At the same specificity (95%), total analysis had 80% sensitivity ($P = 0.30$ compared with sectoral analysis; Fig. 5B and Table 3). With Group 2, sectoral and total analyses with BMO-MRW showed equivalent diagnostic performance ($P =$

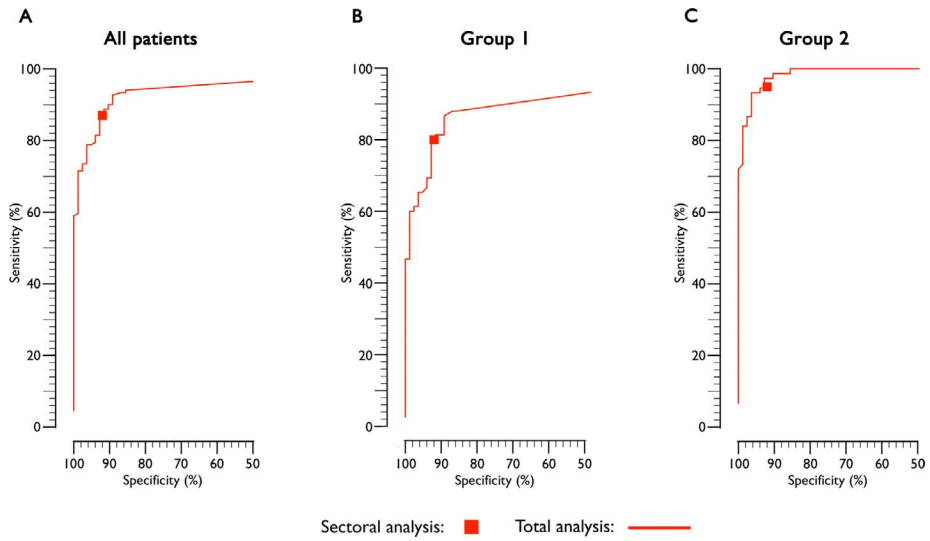

Figure 4. ROC curves obtained from sectoral analysis (discrete points) and total analysis (continuous curves) for all (A), Group 1 (B) and Group 2 (C) patients with BMO-MRW. Data for the total analysis are with the 1% normative limit. Group 1 patients had visual field MD greater than or equal to −3.6 dB and Group 2 patients had MD less than −3.6 dB.

0.48, Fig. 4C). With 1% normative limit and at 92% specificity, sectoral and total analyses yielded 95% and 97% sensitivity, respectively. However, with the 1% normative limit and at 95% specificity, sectoral analysis with RNFLT yielded significantly higher sensitivity (96%) compared with that with the corresponding sensitivity from the total analysis (85%, $P = 0.01$). Results obtained with 5% and 10% normative limits are summarized in Table 2 and Table 3.

The width and depth of BMO-MRW and RNFLT for each glaucoma patient, relative to respective 1% normative limits, ranked according to the degree of visual field damage, are shown in Figure 6. These data show that the most frequent locations for structural damage were the superior and inferior sectors. They also show that most defects were broad enough to be captured by sectoral analysis. For example, 121 (80%) patients had BMO-MRW defects wider than 40°, the smallest sector size considered in sectoral analysis. Similarly, 120 (80%) patients had RNFL defects wider than 40°.

Table 2. Sensitivity and Specificity of Sectoral and Total Analyses With BMO-MRW

Normative Limit	Specificity	Sensitivity (95% Confidence Interval)		
		Sectoral	Total	*P* Value
All patients				
1%	92	87 (82, 92)	88 (83, 93)	0.25
5%	82	94 (90, 98)	96 (93, 99)	0.25
10%	65	96 (93, 99)	97 (94, 100)	0.82
Group 1				
1%	92	80 (71, 89)	81 (72, 90)	0.96
5%	82	88 (81, 95)	92 (86, 98)	0.23
10%	65	93 (87, 99)	94 (89, 99)	1.00
Group 2				
1%	92	95 (90, 100)	97 (93, 100)	0.48
5%	82	100 (–)	100 (–)	1.00
10%	65	100 (–)	100 (–)	1.00

Sensitivity and specificity values shown are percentages.

Discussion

Imaging devices yield large and complex datasets that can be challenging to analyze and interpret. The common strategy of summarizing data into global or sectoral averages for the neuroretinal rim and RNFLT is a practical approach for assimilating such datasets. On the other hand, it is recognized that global averages can fail to detect significant localized damage.[19–21] While sector averages offer a reasonable compromise between data volume and capturing localized damage according to anatomically logical areas, it is not known whether clinically meaningful localized damage can still escape detection with conventional sector-based analysis. We devised a novel method, that we termed total analysis that examines neuroretinal rim and RNFLT data in 1° intervals and can be used to provide a single binary (normal or abnormal) classification. For this reason, our expectation was that total analysis would have better diagnostic accuracy for glaucoma compared with the conventional six (four 40°, one 90°, and one 110°) sectors. Our objective was not to compare rim and RNFLT parameters in their ability to detect glaucoma, but a within-parameter comparison of two methods.

Our results indicated that the diagnostic accuracy with conventional sectoral analysis was at least as good as that with total analysis. These findings were repeatable when patients were divided into groups with less severe (Group 1) and more severe (Group 2) visual field damage. The equivalent diagnostic capability of the two methods was likely due to fact that most rim and RNFL losses were extensive enough to be captured by computing the respective average value in one or more of the conventional sectors. Sectoral damage could be imprecisely captured in the analysis of smaller sectors, or when a localized defect traverses adjacent sectors. In the latter case, the damage may be subthreshold for either sectoral value to fall outside normal limits.

The diagnostic accuracy of both analyses was influenced by the cut-off criterion used to define an abnormal result. With sectoral analysis, we used a fixed arbitrary classification criterion that required average BMO-MRW or RNFLT values in one or more sectors to be outside its respective normal limit to yield a classification of abnormality. A more conservative criterion would result in loss of sensitivity and a gain in

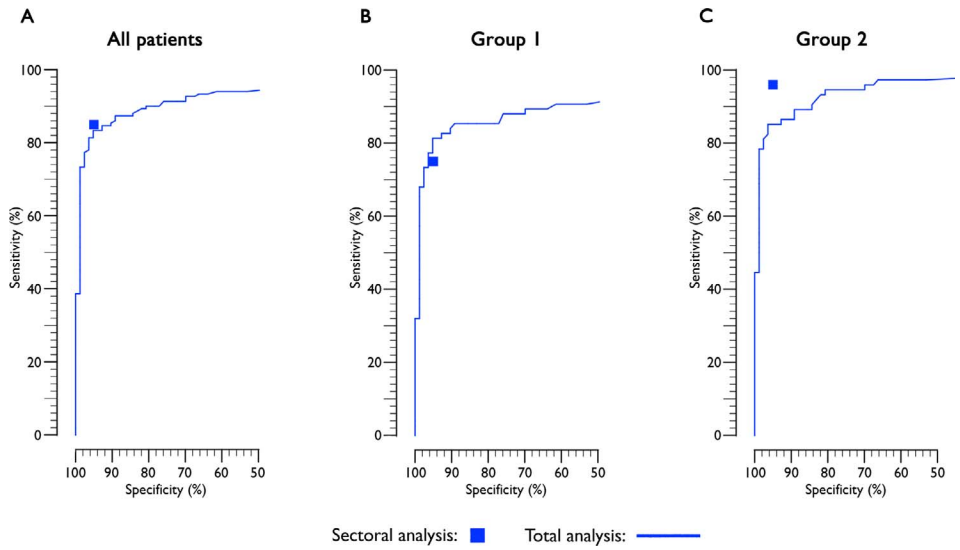

FIGURE 5. ROC curves obtained from sectoral analysis (discrete points) and total analysis (continuous curves) for all (A), Group 1 (B) and Group 2 (C) patients with RNFLT. Data for the total analysis are with the 1% normative limit. Group 1 patients had visual field MD greater than or equal to −3.6 dB and Group 2 patients had MD less than −3.6 dB.

specificity. For example, with the criterion used in the present study, we obtained a sensitivity of 87% and specificity of 92% for sectoral analysis with BMO-MRW. Requiring two or more sectors to be outside the normal limits would have yielded a sensitivity of 75% and specificity of 96%. As we had no previous experience with total analysis, we analyzed the spectrum of cut-off points with ROC analysis. Expectedly, more conservative criteria resulted in gain in specificity and loss of sensitivity. For example, the 10% cut-off criterion (i.e., 10% of more of the measured values had to be outside normal limits to yield a classification of abnormality) yielded a sensitivity of 84% and a specificity of 93% with BMO-MRW. With the 30% cut-off criterion, the respective sensitivity and specificity values were 66% and 98%.

On average, diagnostic performance was better in Group 2 compared with Group 1 for both sectoral and total analyses. This result was expected as diagnostic performance is dependent on disease severity,[30,31] which in our study was expressed as a function of visual field damage. In total analysis, the cut-off criterion is adjustable to attain a good balance between sensitivity and specificity. However, in Group 1, there was no cut-off value in total analysis that was able to attain 100% sensitivity (Figs. 4B, 5B), indicating that a small number of patients had normal BMO-MRW or RNFLT that were within normal limits for all 360 locations (Fig. 6). While we showed equivalent diagnostic accuracy of the two methods in this specific study sample, it is conceivable that total analysis could yield more favorable results at an earlier stage glaucoma where current methods still report results within normative limits. Careful longitudinal study would be required to test this hypothesis.

TABLE 3. Sensitivity and Specificity of Sectoral and Total Analyses With RNFLT

Normative Limit	Specificity	Sensitivity (95% Confidence Interval)		
		Sectoral	Total	*P* Value
All patients				
1%	95	85 (79, 91)	83 (77, 89)	0.54
5%	76	91 (86, 96)	90 (85, 95)	0.80
10%	48	96 (93, 99)	95 (92, 98)	0.75
Group 1				
1%	95	75 (65, 85)	80 (71, 89)	0.30
5%	76	84 (76, 92)	89 (82, 96)	0.34
10%	48	92 (86, 98)	94 (89, 99)	0.68
Group 2				
1%	95	96 (92, 100)	85 (77, 93)	0.01
5%	76	98 (95, 100)	90 (83, 97)	0.04
10%	48	100 (–)	95 (90, 100)	0.13

Sensitivity and specificity values shown are percentages.

In a previous study,[9] we reported overlapping 95% confidence intervals of areas under the ROC curves of BMO-MRW and RNFLT, however, interestingly the means were always higher with BMO-MRW. In the present study, a similar comparison cannot be made. The sensitivity estimates of the total analysis were derived at the fixed specificity level of the sectoral analysis. The latter were nonidentical for BMO-MRW and RNFLT. For example, for the 1% normative limit, the respective values were 92% and 95%. Even assuming these values were identical, the 95% confidence intervals of the sensitivity estimates for BMO-MRW and RNFLT overlapped widely (Tables 2, 3).

Our study had the following limitations: (1) differences in diagnostic accuracy would be expected depending on the severity of glaucomatous damage, referral source for study patients and criteria used to define glaucoma. For example, if the initial diagnosis of glaucoma were biased more toward structural rather than visual field damage, then the diagnostic performance of these methods of OCT analysis would be higher. Furthermore, our study design may have had preferential inclusion of patients with ONH damage compared with RNFLT loss. However, since our study undertook a within-parameter and not a between-parameter comparison, we do not believe that any selection bias favoring inclusion of patients with rim loss would alter the conclusions, (2) our study is limited by the fact that the optimal cut-off criteria for both sectoral and total analysis derived were not independently validated in another data set, however, they do provide a valid comparative analysis between the two methods, and

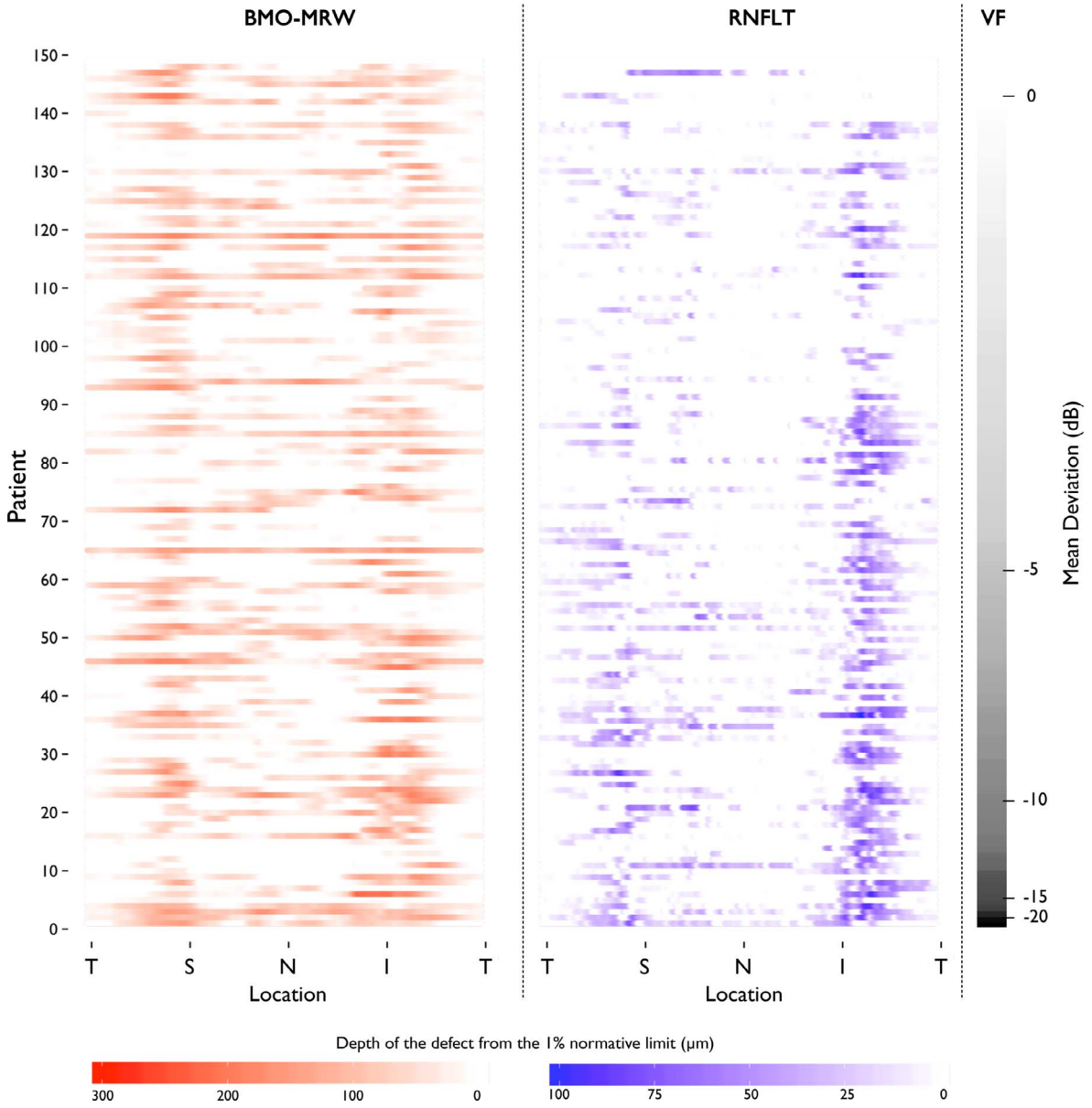

FIGURE 6. Width and depth of BMO-MRW and RNFLT loss compared at the 1% normative limit for each glaucoma patient. Individual patient profiles (*horizontally*) are shown at each of 360 measurement points. Profiles are ordered vertically by visual field MD, indicated by the *gray scale*. T, temporal; S, superior; N, nasal; I, inferior.

(3) the number of measurement locations of BMO-MRW was considerably smaller than that for RNFLT (48 compared with 768). Consequently the interpolation performed at every degree for BMO-MRW could have been inaccurate, especially if there were intervening areas between measurement locations with blood vessels or much localized rim loss. Therefore, it is possible that the diagnostic performance of total analysis for BMO-MRW, but not RNFLT, could have been underestimated.

In summary, irrespective of the degree of visual field damage in this cohort of patients, conventional sector based analysis was able to detect glaucomatous defects at least as well as total analysis with equivalent specificity. Our results indicate that both rim and RNFL loss were broad and deep enough to be captured by conventional sector-based analysis.

Acknowledgments

Supported by grants from the Canadian Institutes of Health Research, Ottawa, Ontario, Canada (MOP11357), the Dalhousie Medical Research Foundation, Halifax, Nova Scotia, Canada, and equipment and unrestricted research support from Heidelberg Engineering GmbH, Heidelberg, Germany.

Disclosure: **V.M. Danthurebandara**, None; **J.R. Vianna**, None; **G.P. Sharpe**, None; **D.M. Hutchison**, None; **A.C. Belliveau**, None; **L.M. Shuba**, None; **M.T. Nicolela**, None; **B.C. Chauhan**, Heidelberg Engineering (F, C, R), Allergan (C, R)

References

1. Reis ASC, Sharpe GP, Yang H, Nicolela MT, Burgoyne CF, Chauhan BC. Optic disc margin anatomy in patients with glaucoma and normal controls with spectral domain optical coherence tomography. *Ophthalmology*. 2012;119:738–747.

2. Srinivasan VJ, Adler DC, Chen Y, et al. Ultrahigh-speed optical coherence tomography for three-dimensional and en face imaging of the retina and optic nerve head. *Invest Ophthalmol Vis Sci*. 2008;49:5103–5110.
3. Strouthidis NG, Grimm J, Williams GA, Cull GA, Wilson DJ, Burgoyne CF. A comparison of optic nerve head morphology viewed by spectral domain optical coherence tomography and by serial histology. *Invest Ophthalmol Vis Sci*. 2010;51:1464–1474.
4. Lee EJ, Kim T-W, Weinreb RN, Park KH, Kim SH, Kim DM. Visualization of the lamina cribrosa using enhanced depth imaging spectral-domain optical coherence tomography. *Am J Ophthalmol*. 2011;152:87–95, e1.
5. Burgoyne CF, Downs JC, Bellezza AJ, Hart RT. Three-dimensional reconstruction of normal and early glaucoma monkey optic nerve head connective tissues. *Invest Ophthalmol Vis Sci*. 2004;45:4388–4399.
6. Reis ASC, O'Leary N, Yang H, et al. Influence of clinically invisible, but optical coherence tomography detected, optic disc margin anatomy on neuroretinal rim evaluation. *Invest Ophthalmol Vis Sci*. 2012;53:1852–1860.
7. Povazay B, Hofer B, Hermann B, et al. Minimum distance mapping using three-dimensional optical coherence tomography for glaucoma diagnosis. *J Biomed Opt*. 2007;12:41204.
8. Chen TC. Spectral domain optical coherence tomography in glaucoma: qualitative and quantitative analysis of the optic nerve head and retinal nerve fiber layer (an AOS thesis). *Trans Am Ophthalmol Soc*. 2009;107:254–281.
9. Chauhan BC, O'Leary N, Almobarak FA, et al. Enhanced detection of open-angle glaucoma with an anatomically accurate optical coherence tomography-derived neuroretinal rim parameter. *Ophthalmology*. 2013;120:535–543.
10. Gardiner SK, Ren R, Yang H, Fortune B, Burgoyne CF, Demirel S. A method to estimate the amount of neuroretinal rim tissue in glaucoma: comparison with current methods for measuring rim area. *Am J Ophthalmol*. 2014;157:540–549, e2.
11. Danthurebandara VM, Sharpe GP, Hutchison DM, et al. Enhanced structure-function relationship in glaucoma with an anatomically and geometrically accurate neuroretinal rim measurement. *Invest Ophthalmol Vis Sci*. 2014;56:98–105.
12. Zako M, Gosho M, Mizumoto K. Correlation between optic nerve head structural parameters and glaucomatous visual field indices. *Clin Ophthalmol*. 2014;8:1203.
13. Pollet-Villard F, Chiquet C, Romanet J-P, Noel C, Aptel F. Structure-function relationships with spectral-domain optical coherence tomography retinal nerve fiber layer and optic nerve head measurements. *Invest Ophthalmol Vis Sci*. 2014;55:2953–2962.
14. Garway-Heath DF, Poinoosawmy D, Fitzke FW, Hitchings RA. Mapping the visual field to the optic disc in normal tension glaucoma eyes. *Ophthalmology*. 2000;107:1809–1815.
15. Garas A, Vargha P, Holló G. Reproducibility of retinal nerve fiber layer and macular thickness measurement with the RTVue-100 optical coherence tomograph. *Ophthalmology*. 2010;117:738–746.
16. Hougaard JL, Heijl A, Bengtsson B. Glaucoma detection using different Stratus optical coherence tomography protocols. *Acta Ophthalmol Scand*. 2007;85:251–256.
17. Shin JW, Uhm KB, Lee WJ, Kim YJ. Diagnostic ability of retinal nerve fiber layer maps to detect localized retinal nerve fiber layer defects. *Eye (Lond)*. 2013;27:1022–1031.
18. Wu H, de Boer JF, Chen TC. Reproducibility of retinal nerve fiber layer thickness measurements using spectral domain optical coherence tomography. *J Glaucoma*. 2011;20:470–476.
19. Lee EJ, Kim T-W, Park KH, Seong M, Kim H, Kim DM. Ability of Stratus OCT to detect progressive retinal nerve fiber layer atrophy in glaucoma. *Invest Ophthalmol Vis Sci*. 2009;50:662–628.
20. Kim NR, Lee ES, Seong GJ, Choi EH, Hong S, Kim CY. Spectral-domain optical coherence tomography for detection of localized retinal nerve fiber layer defects in patients with open-angle glaucoma. *Arch Ophthalmol*. 2010;128:1121–1128.
21. Hwang YH, Kim YY, Kim HK, Sohn YH. Ability of cirrus high-definition spectral-domain optical coherence tomography clock-hour, deviation, and thickness maps in detecting photographic retinal nerve fiber layer abnormalities. *Ophthalmology*. 2013;120:1380–1387.
22. Nukada M, Hangai M, Mori S, et al. Imaging of localized retinal nerve fiber layer defects in preperimetric glaucoma using spectral-domain optical coherence tomography. *J Glaucoma*. 2014;23:150–159.
23. Yoo YC, Park KH. Comparison of sensitivities for detecting diffuse and localized retinal nerve fiber layer defects with time-domain optical coherence tomography in patients with glaucoma. *J Glaucoma*. 2012;22:1.
24. Chauhan BC, Danthurebandara VM, Sharpe GP, et al. Bruch's membrane opening-minimum rim width and retinal nerve fibre layer thickness in a normal white population. A multicentre study. *Ophthalmology*. In press.
25. He L, Ren R, Yang H, et al. Anatomic vs. acquired image frame discordance in spectral domain optical coherence tomography minimum rim measurements. *PLoS One*. 2014;9:e92225.
26. Amini N, Nowroozizadeh S, Cirineo N, et al. Influence of the disc-fovea angle on limits of RNFL variability and glaucoma discrimination. *Invest Ophthalmol Vis Sci*. 2014;55:7332–7342.
27. Almobarak FA, O'Leary N, Reis ASC, et al. Automated segmentation of optic nerve head structures with optical coherence tomography. *Invest Ophthalmol Vis Sci*. 2014;55:1161–1168.
28. McNemar Q. Note on the sampling error of the difference between correlated proportions or percentages. *Psychometrika*. 1947;12:153–157.
29. *R: A Language and Environment for Statistical Computing*. Version 3.1.1. Vienna, Austria: R Foundation for Statistical Computing; 2014.
30. Medeiros FA, Zangwill LM, Bowd C, Sample PA, Weinreb RN. Influence of disease severity and optic disc size on the diagnostic performance of imaging instruments in glaucoma. *Invest Ophthalmol Vis Sci*. 2006;47:1008–1015.
31. Leite MT, Zangwill LM, Weinreb RN, et al. Effect of disease severity on the performance of cirrus spectral-domain OCT for glaucoma diagnosis. *Invest Ophthalmol Vis Sci*. 2010;51:4104–4109.

Investigative Ophthalmology & Visual Science